EPAPS

(1) Pressure-induced polymerization of (3,3) CNT

Small CNTs can spontaneous turn into polymerized crystalline phases under pressure via a direct or intertube-sliding-assisted cross-linking mechanism [1]. To clarify this point, the corresponding structure, enthalpy and volume changes at 10 GPa are shown in Fig. S1 for (3,3) CNT. Up to step 30, (3,3) CNT retains the circular cross-sectional shape but its cell size is reduced considerably by pressure; around step 33, there is a large enthalpy oscillation caused by the tube sliding and distortion; around step 45, the distorted tubes start to interlink, and around step 60, the polymerized crystalline phase is achieved.

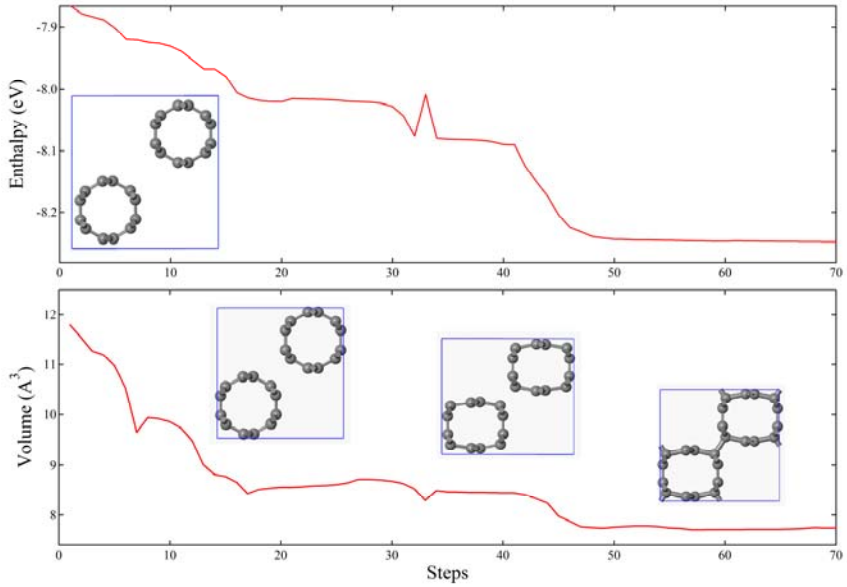

FIG. S1: Enthalpy/volume changes during the spontaneous polymerization transition at 10 GPa for (3,3) CNT. The insets are structural snapshots at 0, 20, 40, and 60 steps.

(2) Competing pathways from polymeric (3,3) CNT toward bct-C_{12} and ign-C_6

For comparison, possible pathways from polymeric (3,3) CNT toward bct-C_{12} and ign-C_6 are also simulated at 10 GPa. As shown in Fig. S2(a), along the pathway toward bct-C_{12}, there are four bond breakings between atoms 6-7, 1-12, 16-17 and 22-23 at step-11, resulting in an enthalpy barrier of 0.30 eV; meanwhile, along the pathway toward ign-C_6 [see Fig. S2(b)], the CNTs are squashed firstly with the tube

rotation and then the squashed CNT-2 inserts into CNT-1 at step 12, resulting in an enthalpy barrier of 0.34 eV. These enthalpy barriers are larger than the values of 0.19-0.22 eV for the pathway toward so-C_{12} [see Fig. S2(c)]. Thus so-C_{12} is energetically more favorable compared to bct-C_{12} and ign-C_6 in terms of the kinetics in the reconstruction pathway.

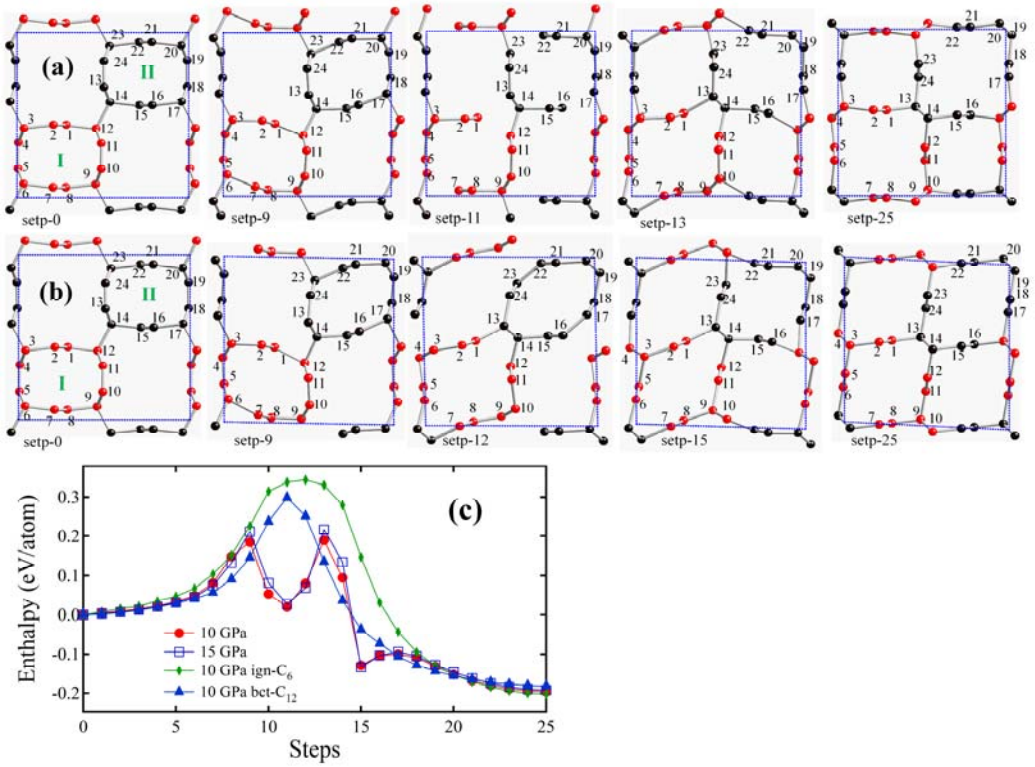

FIG. S2: Pathways from polymeric (3,3) CNT toward bct-C_{12} (a) and ign-C_6 (b) at 10 GPa. The changes of enthalpy versus pathway are plotted in (c).

(3) Surface band structures with C_1 atom chains on the surface

The so-C_{12} structure has two easy-truncation surfaces obtained by bond breaking between the C_1-C_2 bonds in the [010] crystalline direction: one with C_2 and C_3 as the outermost atoms with dangling bonds on sp^3-C_2 sites [Fig. 5(d-f)] and the other with C_1 as the outermost atoms with dangling bonds on the sp^2–type C_1 atoms. The latter structure with dangling bonds on the sp^2–type C_1 atoms is highly unstable with an energy loss of 1.02 eV per surface (or per dangling bond) compared to the former structure. For comparison, the surface band structures with the outermost C_1 atoms are calculated using a 12-layer-thick slab geometry along the [010] crystalline direction

as shown in Fig. S3(c). When the dangling bonds on the sp^2-C_1 atoms are saturated by hydrogen atoms, the π states on C_1 atom chains can be kept and the surface flat band can be outside the surface projected nodal lines [see Fig. S3(b)] similar to that shown in Fig. 5(e). Meanwhile, the surface flat band can be inside the surface projected nodal lines [see Fig. S3(a)] without the dangling bond saturation, similar to the states shown in Fig. 5(d); however, in this case, the bulk bands between the Z and T points deviate from the bulk states due to the strong surface chemical potential. Also surface states along the G-Z and T-Y directions deviate from the projected nodal loop (*a* and *b* points). In Fig. S3(c,d), the partial charge density isosurfaces related to the energy bands around the Fermi level in Fig. S3(a) at the G point and T point are plotted. The electronic charges are located on the topmost surface carbon layers in Fig. S3(c), confirming that the surface flat band inside between two separated nodal lines is derived from the surface atoms. Meanwhile the charges in Fig. S3(d) come from the bulk carbon atoms, confirming bulk band states between Z and T points in Fig. S3(a).

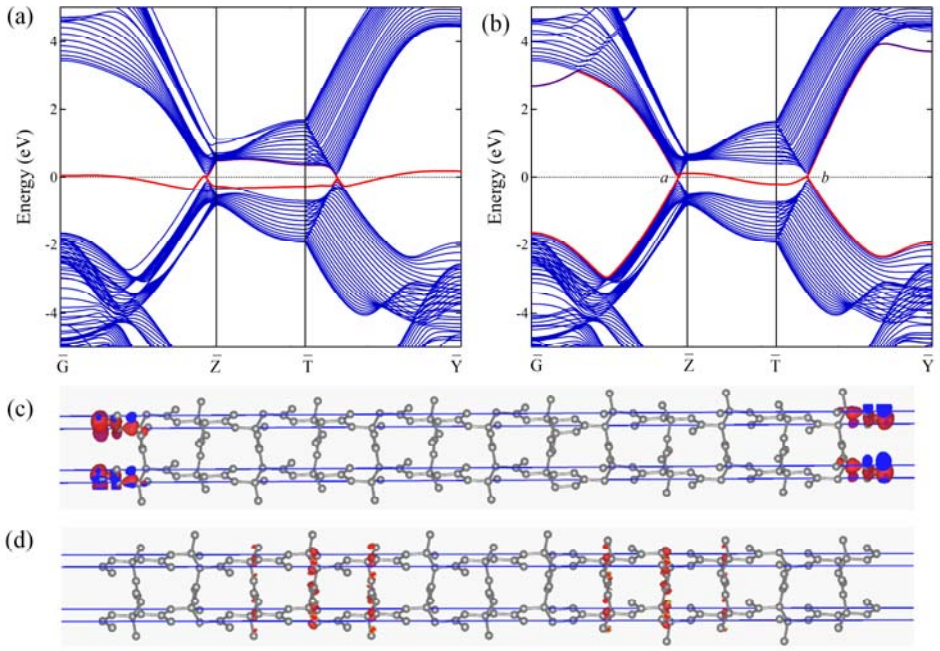

FIG. S3: Surface band structures with C_1 atoms on the topmost surface. The surface flat band (red line) can be inside (a) or outside (b) the surface projected nodal lines, depending on the termination of the surface without (a) or with (b) saturation by hydrogen atoms. (c) Partial charge density isosurfaces (0.05 e/Å^3) related to the (red) surface bands in (a) at the G point. (d) Partial charge density isosurfaces related to the (red) bulk bands in (a) at the T point.

(4) Tight-binding model and Berry phase calculation

As shown in Fig. 5(c), the nodal line structures are mainly composed of *p* orbits of C_1 and C_3 atoms. The tight-binding (TB) Hamiltonians in the basis of the *p* orbits of C_1 and C_3 atoms can be constructed based on the maximally localized Wannier function [2] using Wannier90 [3]. The calculated TB band structures are plotted in Fig. S4(a), which agrees rather well with first-principles DFT results near the Fermi level. Furthermore, Berry phase is calculated by two methods: (1) choosing two lines (the black dash lines) in k_y direction passing through the BZ inside or outside of the area between two separated nodal lines [see Fig. S4(b)], and the Berry phase of the lines inside and outside are calculated to be 0 and π, respectively; (2) choosing a closed loop surrounding one of the nodal lines [see Fig. S4(c)], and the Berry phase surrounding the nodal lines is calculated to be π. These nonzero quantized Berry phase further confirms the topological nodal-line feature in so-C_{12} carbon.

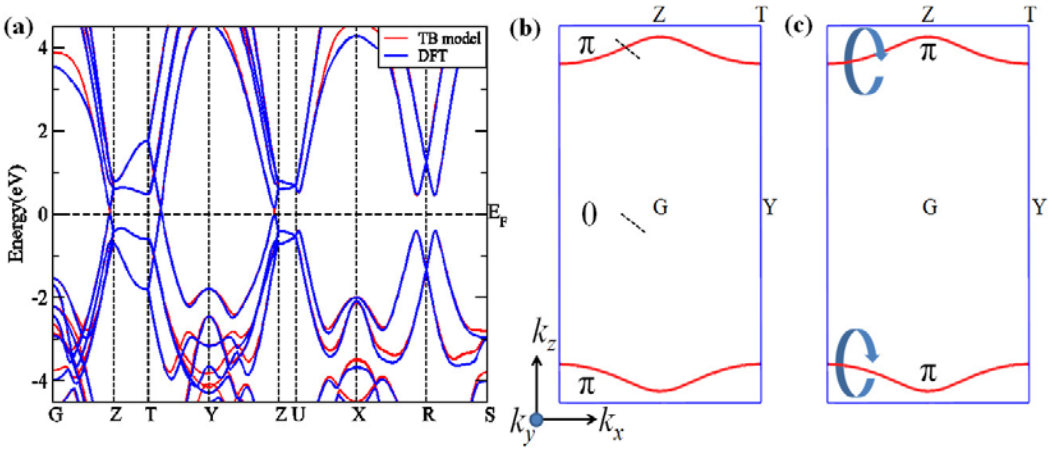

FIG. S4: (a) Bulk band structures of so-C_{12} calculated by DFT and TB model. (b) Berry phase using two lines (the black dash lines) in k_y direction passing through the BZ inside or outside between two separated nodal lines. (c) Berry phase with a closed loop surrounding one of the nodal lines.

References

[1] C. S. Lian and J. T. Wang, J. Chem. Phys. **140**, 204709 (2014).
[2] Q. Wu, S. Zhang, H.-F. Song, M. Troyer, and A. A. Soluyanov, arXiv:1703.07789.
[3] A. A. Mostofi, J. R. Yates, Y.-S. Lee, I. Souza, D. Vanderbilt, and N. Marzari, Comput. Phys. Commun. **178**, 685 (2008).